Supporting Information

A Belt-Like One-Dimensional Dy Chain Exhibiting Slow Magnetic Relaxation Behavior

Zhi Chen,*[a,e] Yanhua Lan,[b] Chenliang Su,[a] Yi-Quan Zhang*,[c] and Wolfgang Wernsdorfer[b,d,e]

[a] *International Collaborative Laboratory of 2D Materials for Optoelectronics Science and Technology of Ministry of Education, College of Optoelectronic Engineering, Shenzhen University, Shenzhen 518060, China. E-mail:zhi.chen@szu.edu.cn*
[b] *Laboratoire Louis Néel–CNRS, BP 166, 25 Avenue des Martyrs, 38042 Grenoble Cedex 9, France*
[c] *Jiangsu Key Laboratory for NSLSCS, School of Physical Science and Technology, Nanjing Normal University, Nanjing 210023, China. E-mail: zhangyiquan@njnu.edu.cn*
[d] *Physikalisches Institut, Karlsruhe Institute of Technology (KIT), Wolfgang-Gaede Str. 1, D-76131, Karlsruhe, Germany*
[e] *Institut for Nanotechnology, Karlsruhe Institute of Technology (KIT), Hermann-von-Helmholtz Platz 1, D-76344, Eggenstein-Leopoldshafen, Germany*

Computational details

Complex **1** is one-dimensional chain including three types of Dy^{III} fragments, and thus we need to calculate three individual Dy^{III} fragments. Complete-active-space self-consistent field (CASSCF) calculations on three individual Dy^{III} fragments of the model structures (see Figure S1 for the calculated model structures of **1**(**Dy1**), **1**(**Dy2**) and **1**(**Dy3**)) extracted from the compound on the basis of single-crystal X-ray determined geometry have been carried out with MOLCAS 8.2 program package.[S1] For Dy^{III} fragments of complex **1**, the influence of the neighboring Dy^{III} ions were taken into account by the closed-shell La^{III} *ab initio* embedding model potentials (AIMP; La.ECP.deGraaf.0s.0s.0e-La-(LaMnO3.).[S2]

The basis sets for all atoms are atomic natural orbitals from the MOLCAS ANO-RCC library: ANO-RCC-VTZP for Dy^{III} ion; VTZ for close O and N; VDZ for distant atoms. The calculations employed the second order Douglas-Kroll-Hess Hamiltonian, where scalar relativistic contractions were taken into account in the basis set and the spin-orbit couplings were handled separately in the restricted active space state interaction (RASSI-SO) procedure. For individual Dy^{III} fragments, active electrons in 7 active spaces include all *f* electrons (CAS(9 in 7)) in the CASSCF calculation. To exclude all the doubts, we calculated all the

roots in the active space. We have mixed the maximum number of spin-free state which was possible with our hardware (all from 21 sextets, 128 from 224 quadruplets, 130 from 490 doublets). Single_Aniso[S3] program was used to obtain the energy levels, ***g*** tensors, m_J values, magnetic axes, *et al.,* based on the above CASSCF/RASSI calculations.

Complementary Drawings

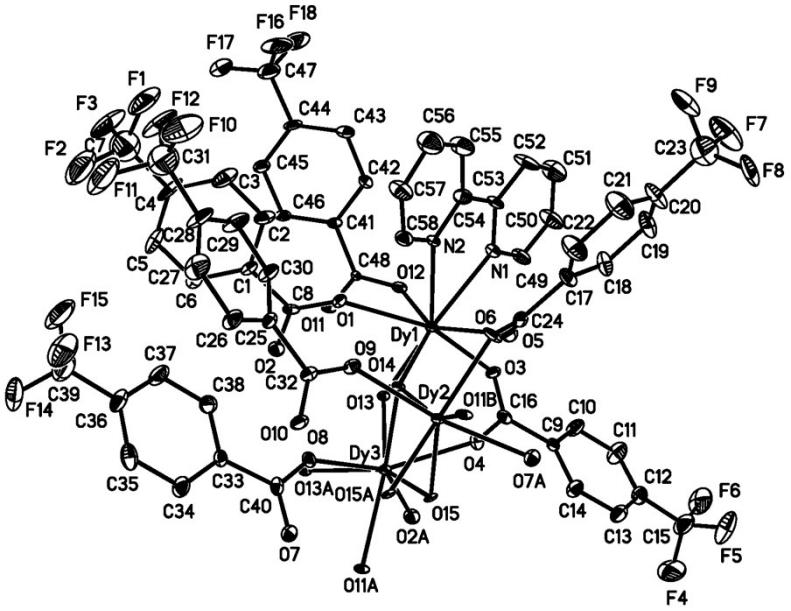

Figure S1. The molecular structure of compound **1**.

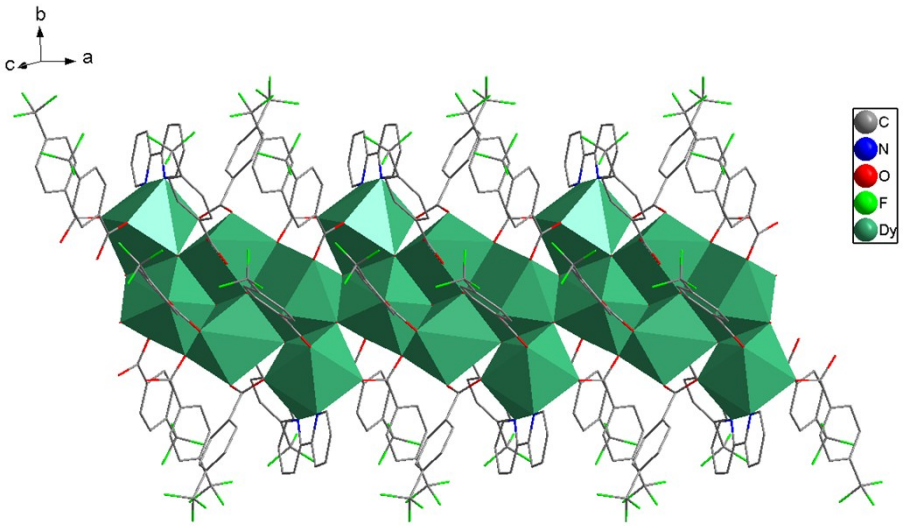

Figure S2. 1D structure of **1**, and its coordination polyhedra of Dy(III) ions.

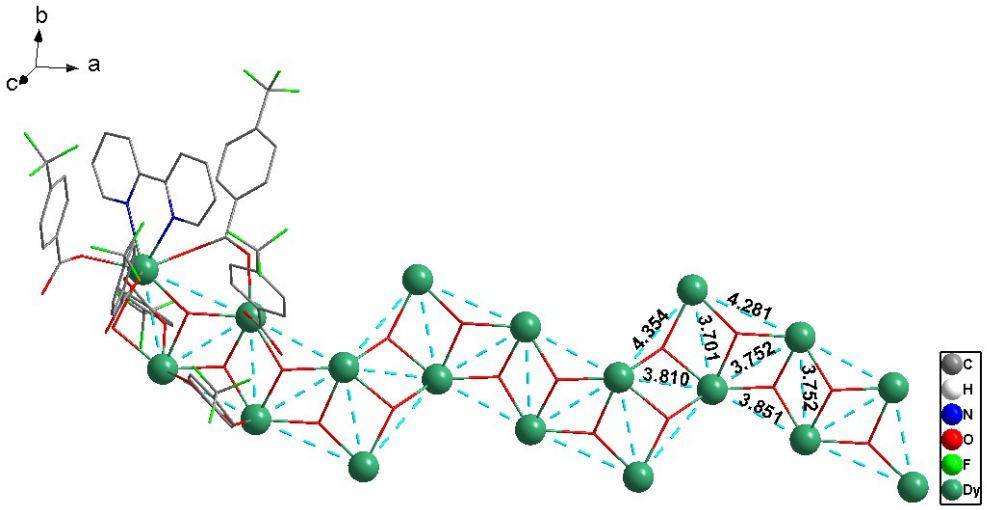

(b)

Figure S3. The Dy···Dy distances in 1D structure of **1**.

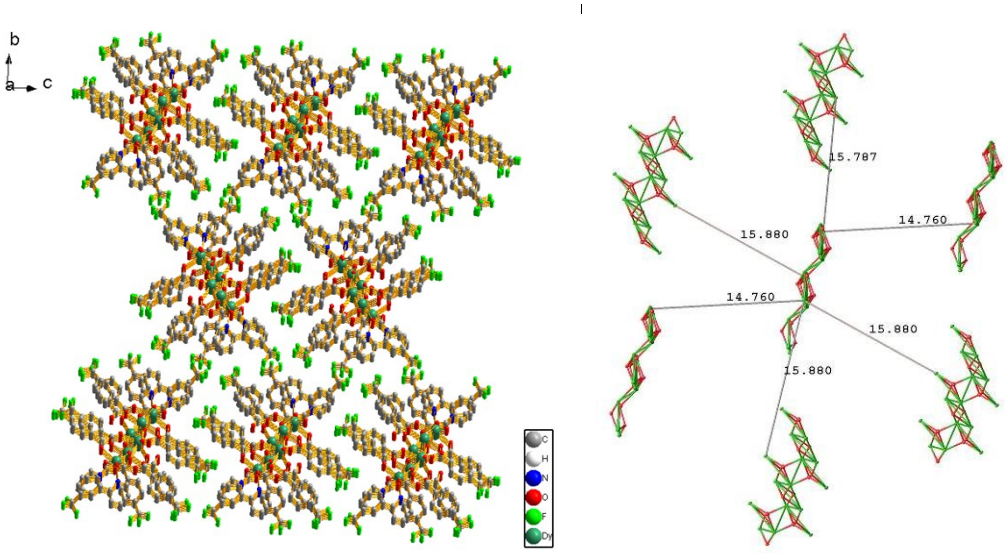

(a) (b)

Figure S4. (a) 3D pack view of compound **1**. (b) the shortest distances of Dy-Dy between adjacent 1D Dy chains.

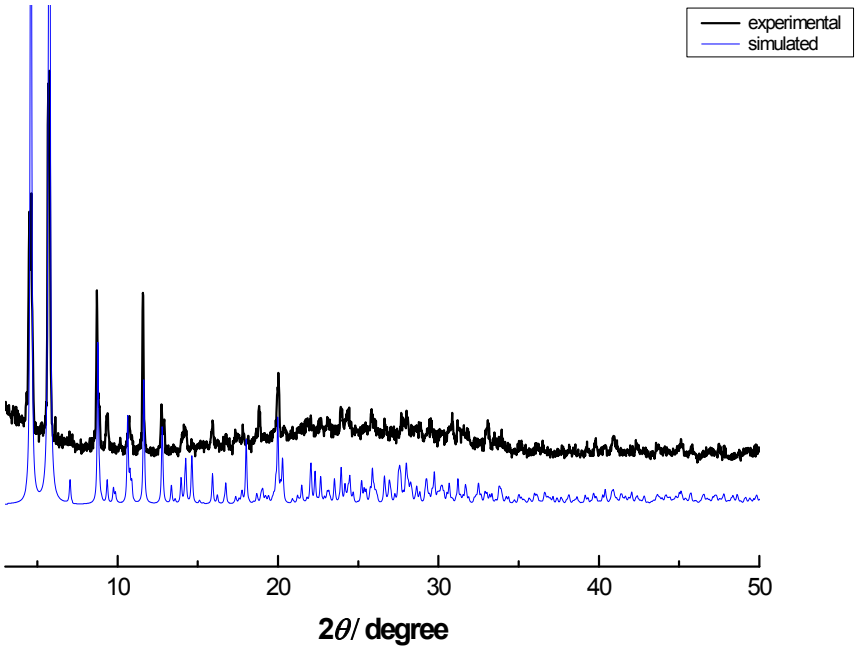

Figure S5. PXRD of compound **1**.

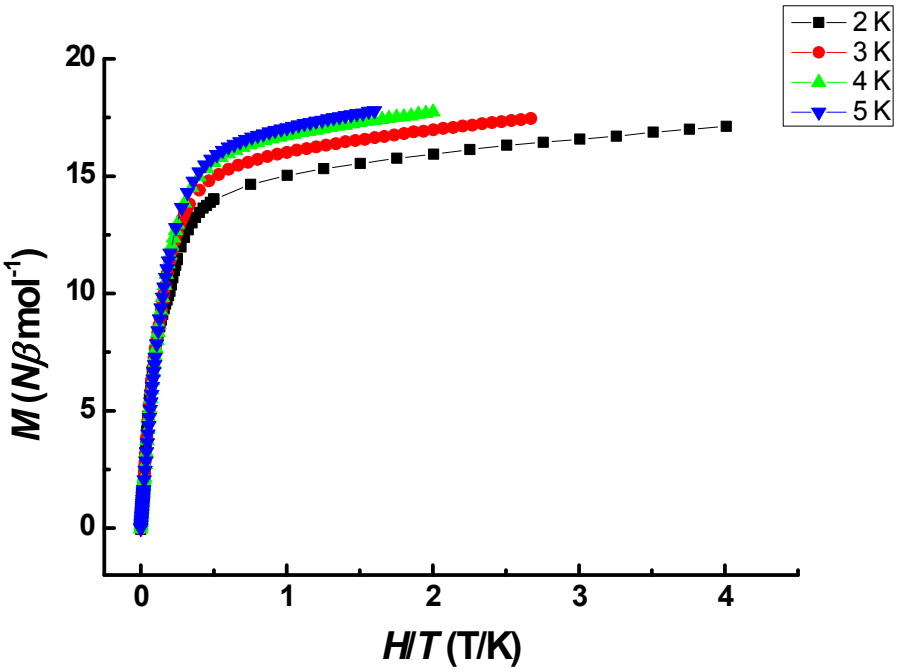

Figure S6. *M* versus *H*/*T* plots of **1** at 2, 3, 4 and 5 K.

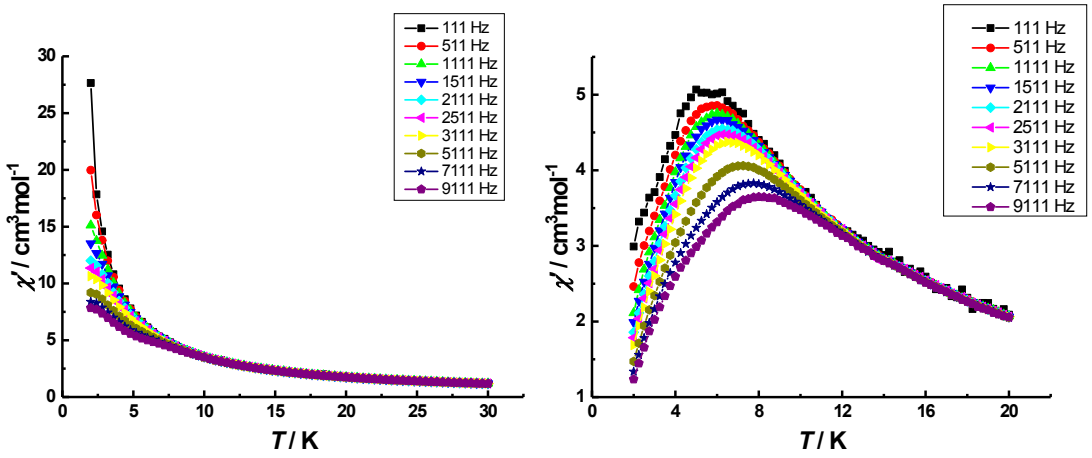

(a) (b)

Figure S7. Plots of χ_M' *vs* temperature for **1** at H_{dc} = 0 (a) and H_{dc} = 5 kOe (b) under indicated frequencies.

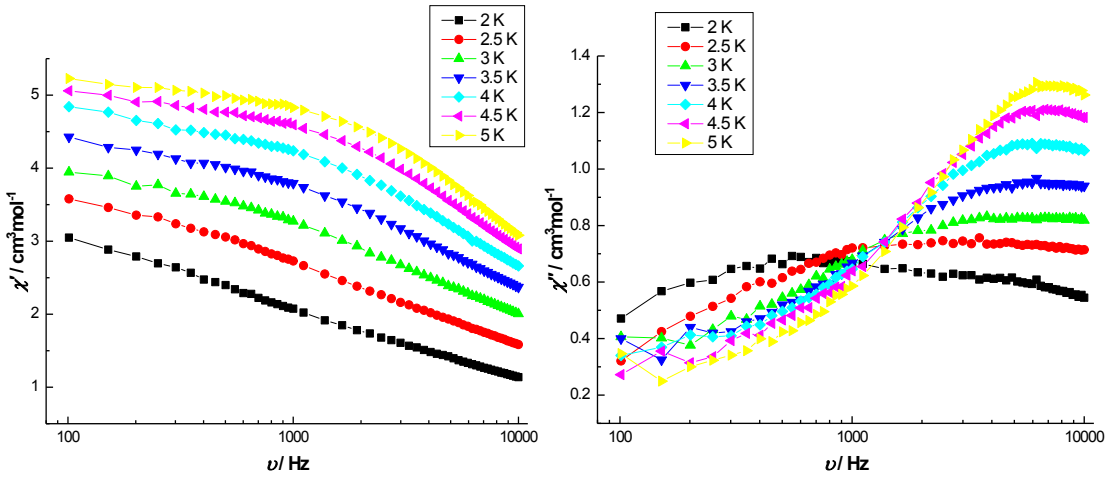

(a) (b)

Figure S8. Plots of χ_M' (a) and χ_M'' (b) *vs* frequencies of **1** at different temperatures.

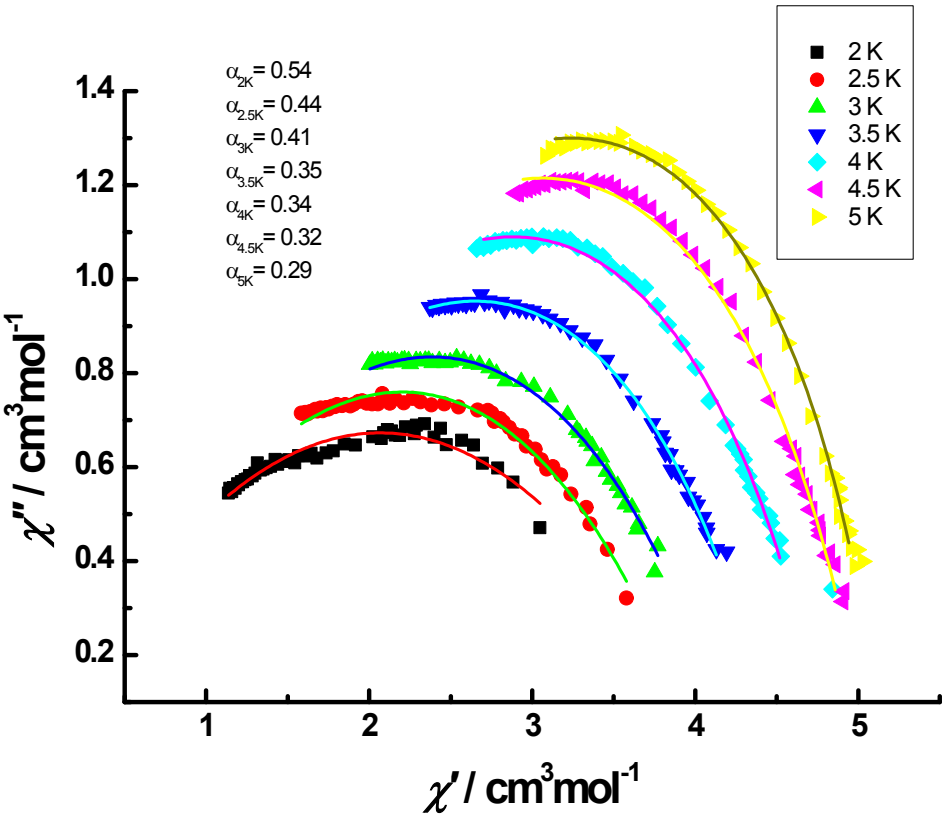

Figure S9. The Cole-Cole Plots of **1.** Solid lines are the least-squares fitting results**.**

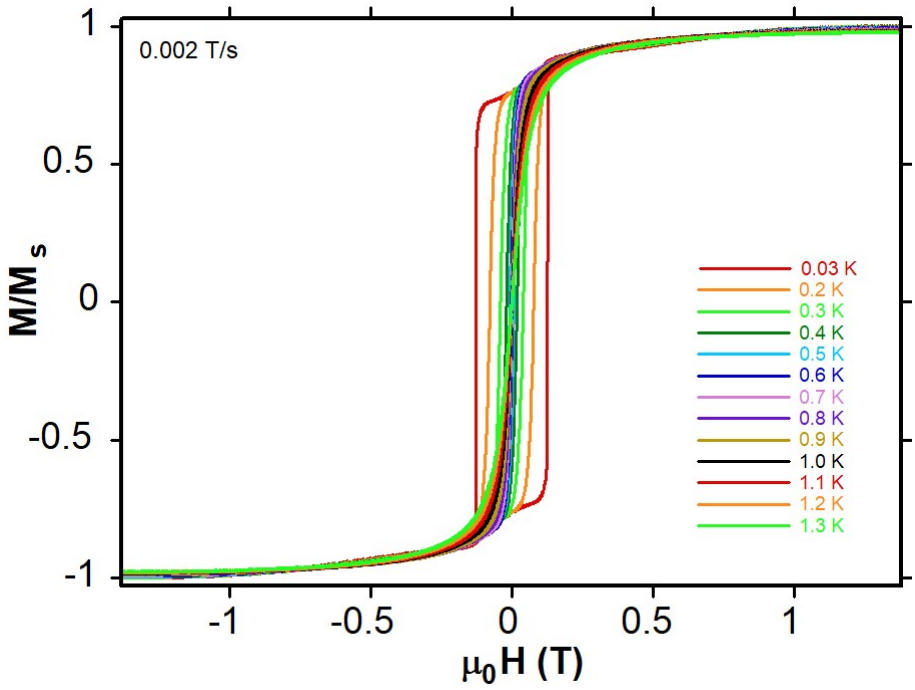

Figure S10. The hysteresis loops of **1** at different temperature measured by Micro-SQUID technique.

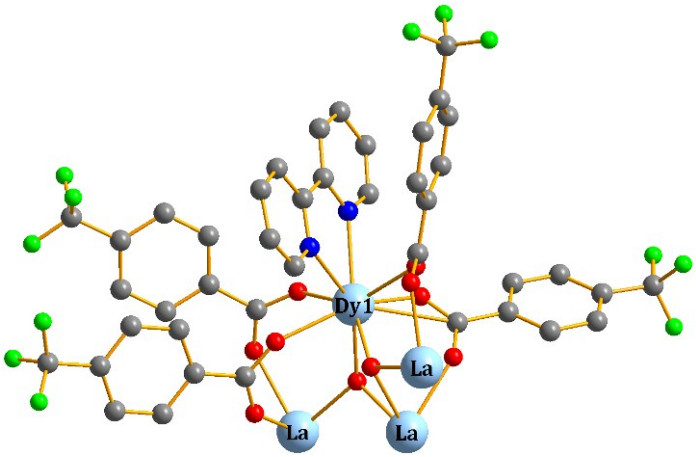

1(Dy1)

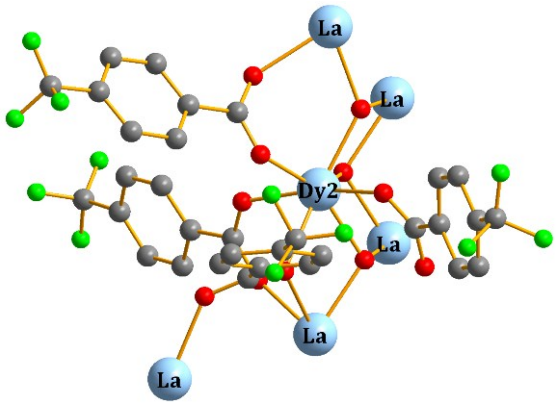

1(Dy2)

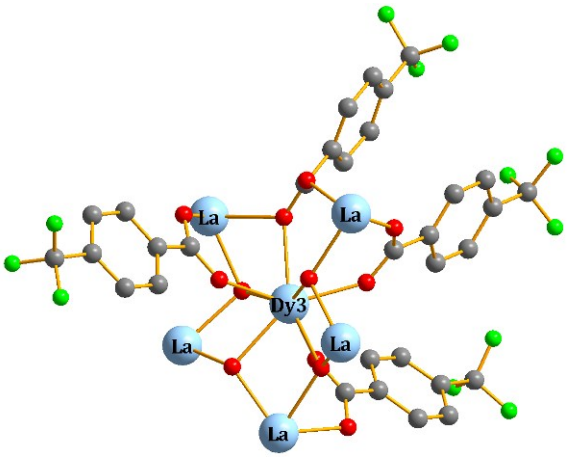

1(Dy3)

Figure S11. Calculated model structures of Dy^{III} fragments of **1**(**Dy1**), **1**(**Dy2**) and **1**(**Dy3**) of complex **1**; H atoms are omitted.

Table S1. Calculated energy levels (cm^{-1}), ***g*** (g_x, g_y, g_z) tensors and m_J values of the lowest

eight Kramers doublets (KDs) of individual Dy^{III} fragments of **1**(**Dy1**), **1**(**Dy2**) and **1**(**Dy3**) of complex **1** using CASSCF/RASSI with MOLCAS 8.2.

KDs	**1**(**Dy1**)			**1**(**Dy2**)			**1**(**Dy3**)		
	E/cm^{-1}	$\boldsymbol{g}$	m_J	E/cm^{-1}	$\boldsymbol{g}$	m_J	E/cm^{-1}	$\boldsymbol{g}$	m_J
1	0.0	0.109 0.199 19.279	±15/2	0.0	0.022 0.038 19.617	±15/2	0.0	0.045 0.093 19.239	±15/2
2	86.2	0.709 1.011 16.001	±13/2	253.2	0.948 2.240 15.271	±13/2	95.6	0.034 0.089 16.931	±13/2
3	141.5	0.351 1.654 14.331	±11/2	360.2	1.127 3.328 14.063	±3/2	215.3	1.274 1.975 13.448	±11/2
4	189.9	3.086 4.690 10.466	±9/2	507.7	8.591 6.019 1.173	±11/2	310.4	3.116 3.799 9.047	±7/2
5	255.7	1.305 5.088 10.184	±5/2	638.1	2.308 4.940 10.625	±7/2	363.5	2.894 3.611 14.148	±5/2
6	307.8	1.748 3.420 13.855	±1/2	762.9	1.970 2.081 13.600	±1/2	439.6	0.050 0.126 14.512	±1/2
7	426.6	0.031 0.104 18.352	±3/2	853.2	0.180 0.427 19.045	±5/2	499.4	0.030 0.041 18.831	±3/2
8	513.0	0.007 0.016 19.390	±7/2	939.9	0.062 0.196 19.153	±9/2	729.9	0.000 0.002 19.662	±9/2

Table S2. Wave functions with definite projection of the total moment | m_J > for the lowest two Kramers doublets (KDs) of individual Dy^{III} fragments of **1**(**Dy1**), **1**(**Dy2**) and **1**(**Dy3**) for complex **1** using CASSCF/RASSI with MOLCAS 8.2.

	E/cm^{-1}	wave functions
1(**Dy1**)	0.0	92%|±15/2>+5%|±11/2>
	86.2	80%|±13/2>+4%|±11/2>+12%|±9/2>
1(**Dy2**)	0.0	98%|±15/2>
	253.2	82%|±13/2>+7%|±7/2>+3%|±5/2>+3%|±3/2>+3%|±1/2>
1(**Dy3**)	0.0	89%|±15/2>+10%|±11/2>
	95.6	70%|±13/2>+11%|±11/2>+15%|±9/2>

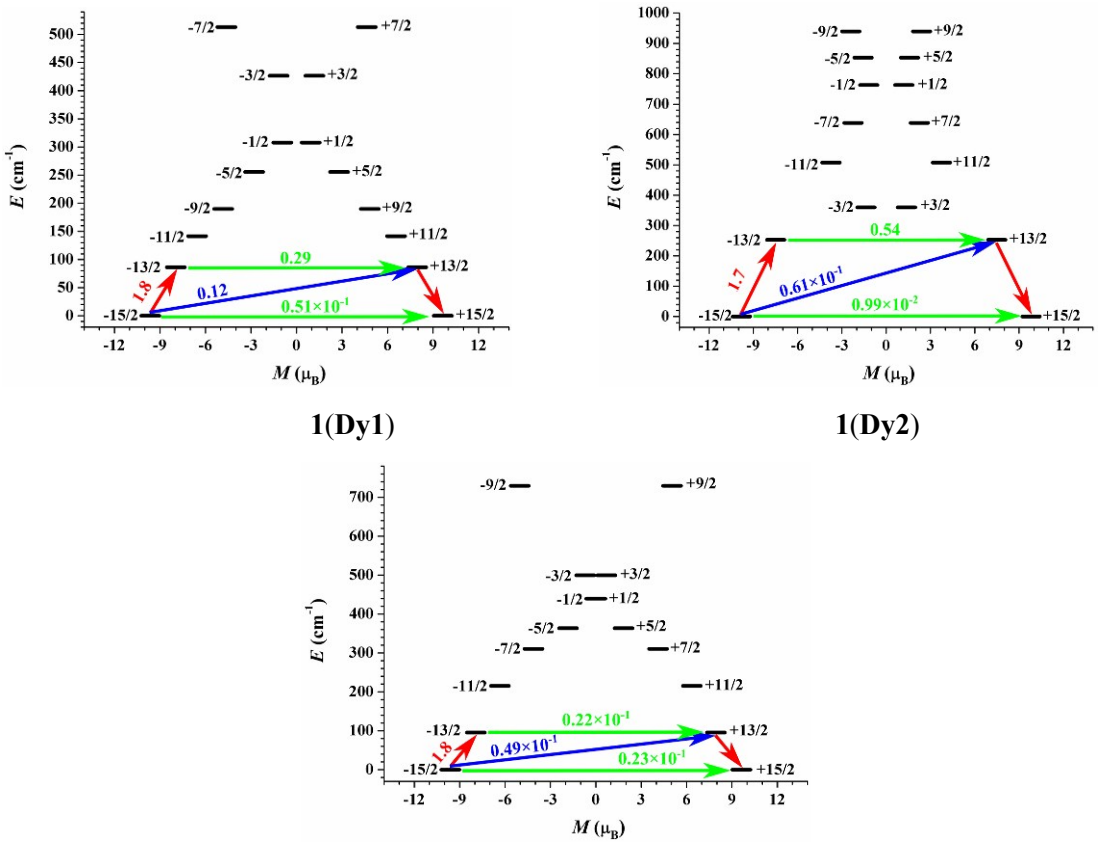

Figure S12. Magnetization blocking barriers for individual Dy^{III} fragments of **1**(**Dy1**), **1**(**Dy2**) and **1**(**Dy3**) in complex **1**. The thick black lines represent the Kramers doublets as a function of their magnetic moment along the magnetic axis. The green lines correspond to diagonal quantum tunneling of magnetization (QTM); the blue line represent off-diagonal relaxation process. The numbers at each arrow stand for the mean absolute value of the corresponding matrix element of transition magnetic moment.

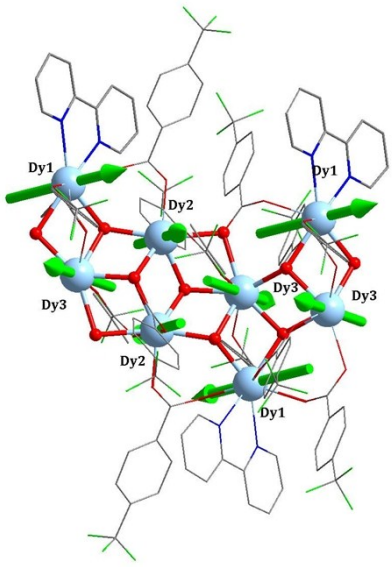

Figure S13. Calculated orientation of the local main magnetic axes of the ground Kramers doublet on Dy^{III} ions of complex **1**.

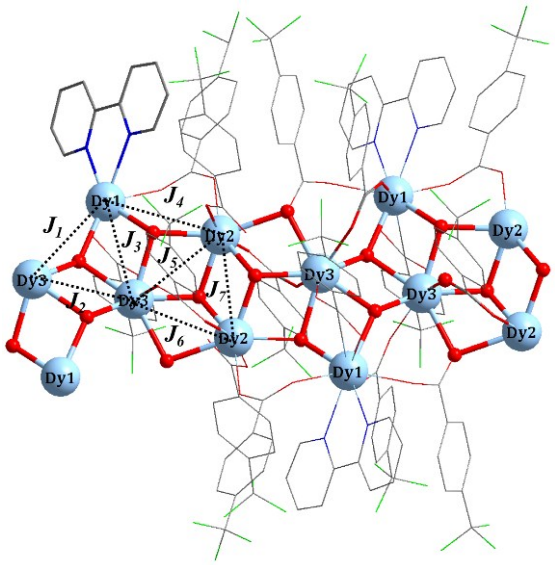

Figure S14. Seven types of J_1, J_2, J_3, J_4, J_5, J_6 and J_7 in complex **1**.

Table S4. Calculated seven dipole-dipole interactions (J_1, J_2, J_3, J_4, J_5, J_6 and J_7) between Dy^{III} ions in complex **1** (cm^{-1}).

J_1	−0.76
J_2	−2.90
J_3	−1.31
J_4	−1.36
J_5	−2.07
J_6	−1.68
J_7	−3.07

References:

S1 (a) Aquilante, F.; De Vico, L.; Ferré, N.; Ghigo, G.; Malmqvist, P.-Å.; Neogrády, P.; Pedersen, T. B.; Pitonak, M.; Reiher, M.; Roos, B. O.; Serrano-Andrés, L.; Urban, M.; Veryazov, V.; Lindh, R. *J. Comput. Chem*., **2010**, *31*, 224. (b) Veryazov, V.; Widmark, P. -O.; Serrano-Andres, L.; Lindh, R.; Roos, B. O. *Int. J. Quantum Chem*., **2004**, *100*, 626. (c) Karlström, G.; Lindh, R.; Malmqvist, P. -Å.; Roos, B. O.; Ryde, U.; Veryazov, V.; Widmark, P. -O.; Cossi, M.; Schimmelpfennig, B.; Neogr´ady, P.; Seijo, L. *Comput. Mater. Sci*., **2003**, *28*, 222.

S2 Seijo, L.; Barandiarán, Z. *Computational Chemistry: Reviews of Current Trends*; World Scientific, Inc.: Singapore, 1999; pp 455−152.

S3 (a) Chibotaru, L. F.; Ungur, L.; Soncini, A. *Angew. Chem. Int. Ed.*, **2008**, *47*, 4126. (b) Ungur, L.; Van den Heuvel, W.; Chibotaru, L. F. *New J. Chem.*, **2009**, *33*, 1224. (c) Chibotaru, L. F.; Ungur, L.; Aronica, C.; Elmoll, H.; Pilet, G.; Luneau, D. *J. Am. Chem. Soc.*, **2008**, *130*, 12445.